



Ruthenium/dendrimer complex immobilized on silica-functionalized magnetite nanoparticles catalyzed oxidation of stilbenes to benzil derivatives at room temperature

Dariush Saberi^{1,2} | Hajar Hashemi³ | Niloofar Ghanaatzadeh³ |

Majid Moghadam⁴ | Khodabakhsh Niknam³

¹Fisheries and Aquaculture Department, College of Agriculture and Natural Resources, Persian Gulf University, Bushehr, 75169, Iran

²Marine Chemistry Department, Faculty of Marine Science and Technology, Persian Gulf University, Bushehr, 75169, Iran

³Department of Chemistry, Faculty of Sciences, Persian Gulf University, Bushehr, 75169, Iran

⁴Catalysis Division, Department of Chemistry, University of Isfahan, Isfahan, 81746-73441, Iran

Correspondence

Dariush Saberi, Fisheries and Aquaculture Department, College of Agriculture and Natural Resources, Persian Gulf University, Bushehr 75169, Iran.
Email: saberi_d@pgu.ac.ir

A new ruthenium/dendrimer complex stabilized on the surface of silica-functionalized nano-magnetite was fabricated and well characterized. The nano-catalyst showed good activity in the synthesis of benzil derivatives via the oxidation of stilbenes with high turnover frequency (TOF) at room temperature. Moreover, the catalyst could also be reused up to fifteen times without any loss of its activity.

KEY WORDS

dendrimer, Diaryl-1,2-diketones, magnetite nanoparticles, oxidation, ruthenium

1 | INTRODUCTION

One of the most significant building blocks in a wide range of natural products and biologically active compounds are 1,2-diketones.^[1] They are also important as a precursor for the synthesis of *N*-heterocyclic carbenes.^[2] Especially, diaryl-1,2-diketones (benzils) have shown an extensive ability as corrosion inhibitors,^[3] photoinitiators,^[4] and antitumors.^[5] Various methods are available in the literatures for the synthesis of benzils, mainly from the oxidation of a suitable precursor^[6] or oxidative-coupling pathways.^[7] Among them, oxidation of alkenes constitutes one of the most straightforward routes towards their synthesis since they are cheaper and more easily available than other precursors. In 2011, Wan *et al.* reported a ruthenium complex catalyzed oxidation of alkenes towards synthesis of α -diketones using

TBHP as an oxidant at room temperature.^[6e] Subsequently, an elegant protocol was reported for synthesis of benzil derivatives by Sun *et al.* at 2013, via oxidation of stilbenes in an I₂-H₂O system.^[6g] It was an acid- and metal-free protocol for this family of compounds, although two equivalent (not catalytic) of iodine was used.

From the view of green chemistry, employment of a recoverable and reusable catalytic system especially when a toxic and costly transition metal (e.g. Pd and Ru) is exploited as the catalyst, has warranted attention since it is desirable from economic and environmental point of view. Moreover, catalytic methods are greener than approaches in which stoichiometric reagents are exploited.

Because of the importance of diaryl-1,2-diketones and taking into account the principles of green

chemistry, we set our minds to introducing a new heterogeneous catalytic system consisting of ruthenium/dendrimer complex immobilized on silica-functionalized magnetite nanoparticles as a highly efficient and magnetically separable catalyst in oxidation of stilbenes to benzil derivatives at room temperature. Dendrimers, are highly branched molecules that can be synthesized in well-defined patterns and sizes (generations) that allow control over molecular weight, topology, cavity size, and surface functionality.^[8] Lately, much attention has been devoted to the synthesis and characterization of variously modified dendrimers because of the numerous potential applications that such materials present. Of the other virtues of this system is its magnetic hallmark which gives rise to easy separation of catalyst from the reaction media and straightforward work-up.

2 | RESULTS AND DISCUSSIONS

2.1 | Experimental

Chemicals, Instrumentation and Analysis.

All reagents were purchased from commercial suppliers and used without further purification. The catalyst was characterized using spectroscopic techniques (FT-IR, inductively coupled plasma (ICP), vibrating sample magnetometry (VSM), thermal gravimetric analysis (TGA), scanning electron microscopy–energy-dispersive X-ray analysis (SEM–EDX) and transmission electron microscopy (TEM)). FT-IR spectra were obtained over the region 400–4000 cm⁻¹ with NICOLET IR100 FT-IR with spectroscopic-grade KBr. Powder X-ray diffraction spectrum was recorded at room temperature by a Philips Xpert 1710 diffractometer using Cu-K α ($\lambda = 1.54056 \text{ \AA}$) in Bragg–Brentano geometry (θ –2 θ). ICP analysis was accomplished using a VISTA-PRO, CCD simultaneous ICP analyzer. Magnetic properties of catalyst were obtained by vibrating sample magnetometer/Alternating Gradient Force Magnetometer (VSM/AGFM, MDK Co, Iran, www.mdk-magnetic.com). TGA was performed on a Thermal Analyzer with a heating rate of 20 °C min⁻¹ over a temperature range of 30–600 °C under flowing compressed N₂. SEM images were observed using Philips XL 30 and S-4160 instruments with gold coating equipped with EDX. TEM measurements were carried out at 120 kV (Philips model CM120). ¹H-NMR and ¹³C-NMR spectra were recorded on a Bruker Avance (DRX 400 MHz) in pure deuterated CDCl₃ solvent with tetramethylsilane (TMS) as internal standard.

3 | CATALYST PREPARATION

3.1 | Preparation of silica-functionalized magnetite nanoparticles (Fe₃O₄@SiO₂)

Silica-coated magnetite nanoparticles were synthesized by a chemical co-precipitation technique of ferric and ferrous ions in alkali solution.^[9] of FeCl₃·6H₂O (5 mmol) and FeCl₂·4H₂O (2.5 mmol) salts were dissolved in 100 ml of deionized water under vigorous stirring (800 rpm). Then NH₄OH solution (25% w/w, 30 ml) was added to the mixture at room temperature. The addition of NH₄OH solution followed to maintain the reaction pH between 11 and 12 at which a black suspension was formed. The resulting black dispersion was continuously stirred for 1 hr at room temperature and then refluxed for another 1 hr. Coating of a layer of silica on the surface of the Fe₃O₄ nanoparticles was achieved by adding ethanol (40 ml) to the purified nanoparticles and heating for 1 hr at 40 °C. Subsequently, tetraethyl orthosilicate (TEOS; 10 ml) was charged to the reaction vessel, the mixture was continuously stirred for 24 hr. The silica-coated nanoparticles (Fe₃O₄@SiO₂) were collected using a magnet, followed by washing five times with EtOH and diethyl ether, respectively, and drying at 100 °C in vacuum for 12 hr.

3.2 | Surface modification of Fe₃O₄@SiO₂ nanoparticles with propylamine groups (Fe₃O₄@SiO₂-PA)

Propylamine groups were stabilized on the surface of Fe₃O₄@SiO₂ nanoparticles based on the previously reported procedure.^[10] The synthesized Fe₃O₄@SiO₂ nanoparticles (1.0 g) was suspended in 50 ml of dry toluene and then an excess of 3-aminopropyltrimethoxysilane (3.0 ml) was added, followed by addition of triethylamine (2.5 ml). The suspension was magnetically stirred and refluxed for 12 hr. The reaction was then stopped and the resultant modified nanoparticles cooled to room temperature, transferred to a vacuum glass filter, and washed with a mixture of toluene, ethanol, deionized water, and eventually with methanol. Fe₃O₄@SiO₂-PA was dried under vacuum at 60 °C for 12 hr.

3.3 | Synthesis of Fe₃O₄@SiO₂-PA-TDIC1

In a 50 ml round bottomed flask was added Fe₃O₄@SiO₂-PA (1.0 g), toluene-2,4-diisocyanate (TDIC) (1.04 g, 6 mmol), THF (10.0 ml) and the reaction mixture stirred

overnight at room temperature. Finally, the resulting nanoparticles were separated using an external magnet, washed with EtOH (3×10 ml) and dried at 60°C for 24 hr.

3.4 | Synthesis of first generation of dendrimer stabilized on the surface of magnetite nanoparticles (G1)

In a 50 ml round bottomed flask was added $\text{Fe}_3\text{O}_4@\text{SiO}_2$ -PA-TDIC1 (1.0 g), pentaerytheritol (0.816 g, 6 mmol), DMF (15.0 ml) and the reaction mixture stirred at 80°C for 24 hr. Finally, the resulting nanoparticles were separated using an external magnet, washed with EtOH (3×10 ml) and dried at 60°C for 24 hr.

3.5 | Synthesis of $\text{Fe}_3\text{O}_4@\text{SiO}_2$ -AP-TDIC₂ via the reaction of toluene-2,4-diisocyanate with G1

In a 50 ml round bottomed flask was added G1 (1.0 g), toluene-2,4-diisocyanate (TDIC) (3.12 g, 18 mmol), THF (10.0 ml) and the reaction mixture stirred at 50°C for 24 hr. Finally, the resulting nanoparticles were separated using an external magnet, washed with EtOH (3×10 ml) and dried at 50°C for 24 hr.

3.6 | Synthesis of second generation of dendrimer stabilized on the surface of magnetite nanoparticles (G2)

In a 50 ml round bottomed flask was added $\text{Fe}_3\text{O}_4@\text{SiO}_2$ -PA-TDIC2 (1.0 g), pentaerytheritol (2.44 g, 18 mmol), DMF (15.0 ml) and the reaction mixture stirred at 80°C for 24 hr. Finally, the resulting nanoparticles were separated using an external magnet, washed with EtOH (3×10 ml) and dried at 60°C for 24 hr.

3.7 | Preparation of dendrimer/ruthenium complex ($\text{Fe}_3\text{O}_4@\text{SiO}_2$ -CD-Ru (III))

In a 50 ml round bottomed flask was added G2 (1.0 g), $\text{RuCl}_3 \cdot x\text{H}_2\text{O}$ (0.2 g, 0.8 mmol), distilled water (10.0 ml) and the reaction mixture stirred at room temperature for 12 hr. Finally, the $\text{Fe}_3\text{O}_4@\text{SiO}_2$ -CD-Ru (III) nanoparticles were separated using an external magnet, washed with distilled water (3×5 ml) and dried at 60°C for 24 hr.

3.8 | General procedure for the synthesis of benzil derivatives

1,2-diarylethene 1 (1 mmol), TBAI (20 mol%, 0.2 mmol), TBHP (5 mmol) and catalyst (5 mg, 0.06 mol% of Ru) were added to a 10 ml Schlenk tube and the mixture stirred at room temperature for 1 hr. The progress of the reaction was monitored by thin-layer chromatography. It was then quenched by an aqueous Na_2SO_3 solution (1 ml), to remove excess TBHP, diluted with ethyl acetate and the catalyst was easily separated from the reaction mixture by using an external magnet and washed twice with EtOAc (3×10 ml). The combined organic layers were dried over Na_2SO_4 , filtered, and evaporated under vacuum. The residue was purified by column chromatography on silica gel (*n*-hexane/ethyl acetate = 20:1) to afford the desired product. All the products were known and gave satisfactory physical and spectral data (melting points, FT-IR, ¹H- and ¹³C-NMR) compared with those reported in the literatures. The spectral data of product **2d**, for example, are as follows:

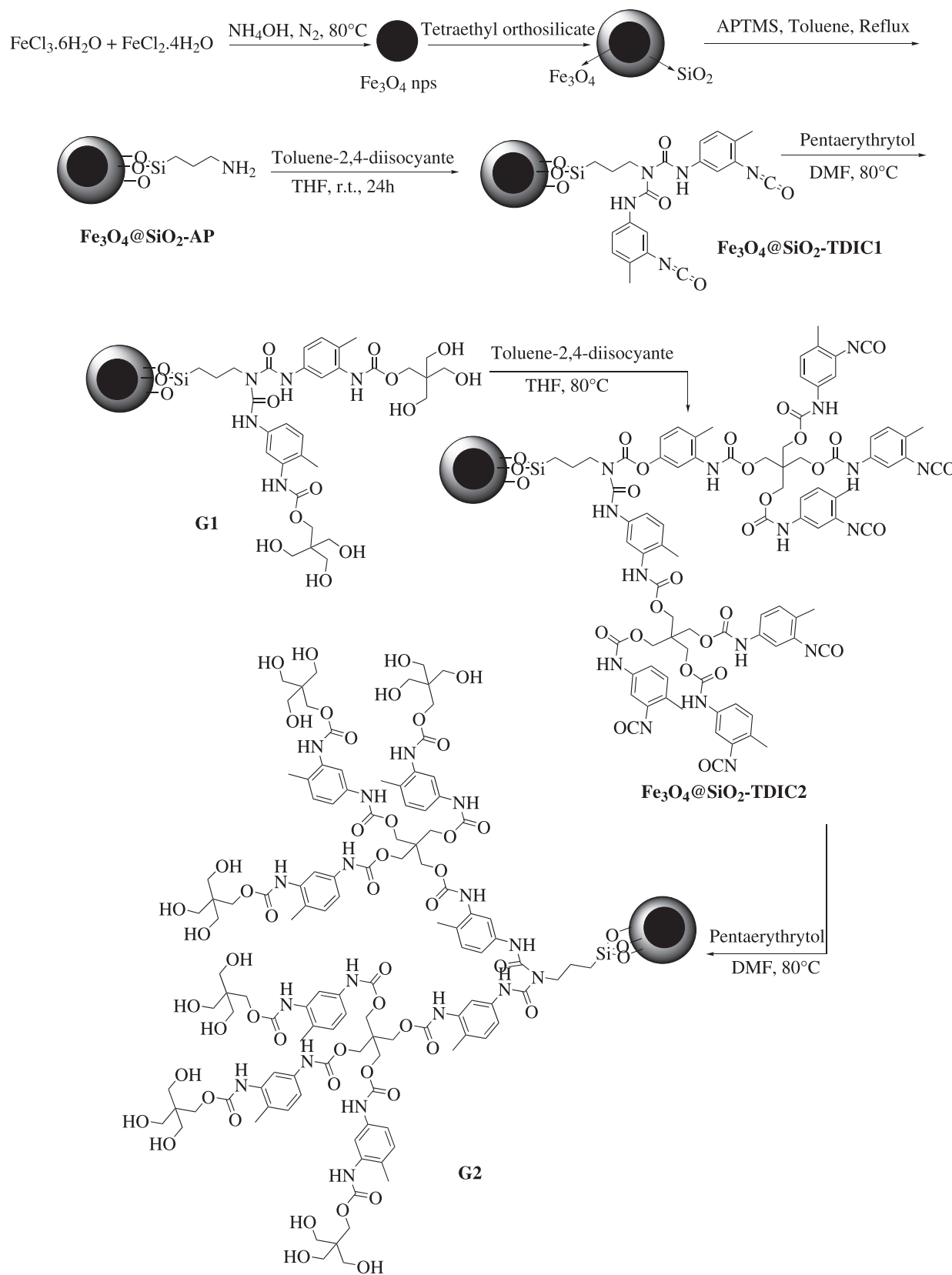
3.9 | 1-(4-methoxyphenyl)-2-phenylethane-1,2-dione (2d)

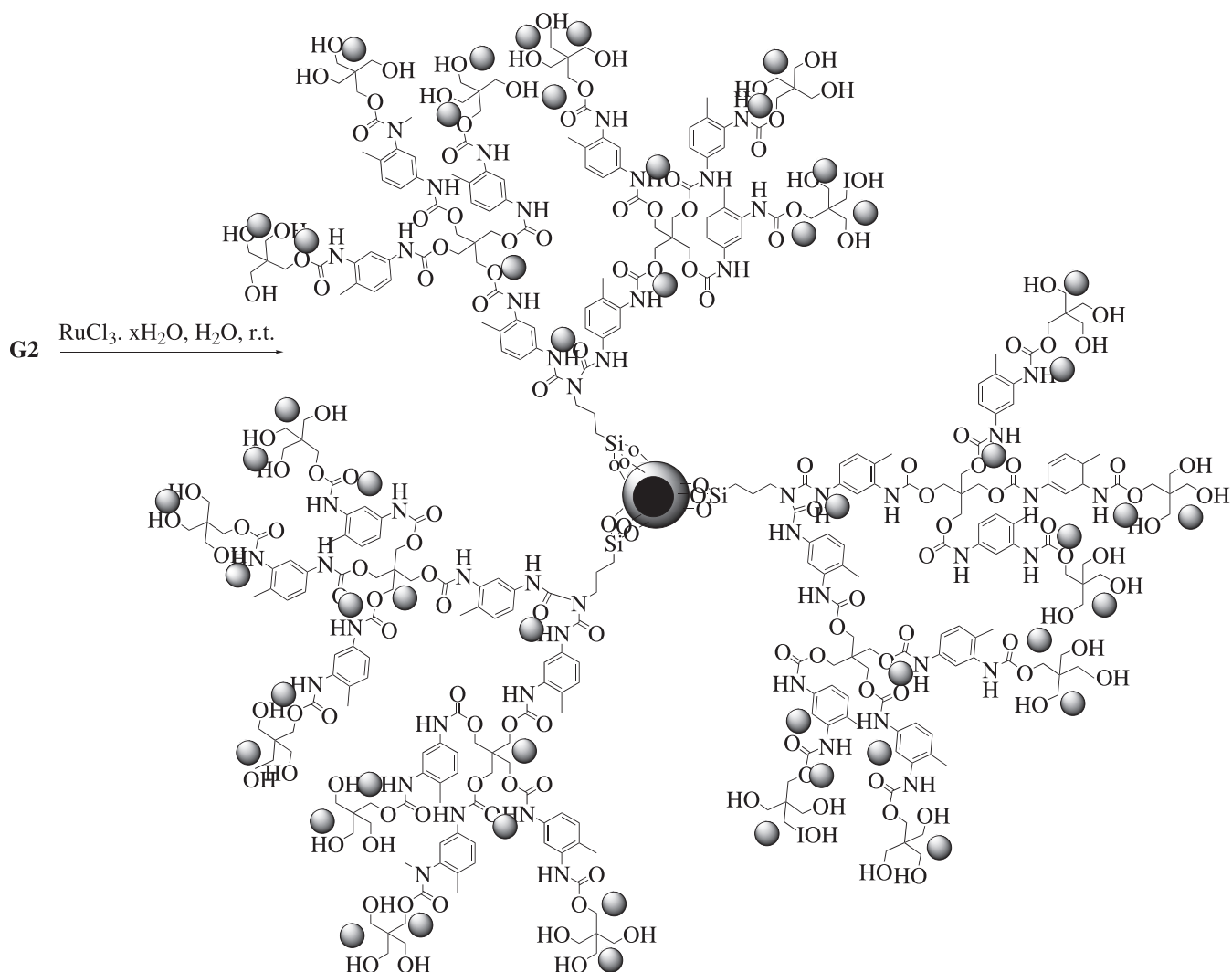
Following the general procedure, the product **2d** was obtained in 82% yield as yellow oil. ¹H-NMR (400 MHz, CDCl_3): δ 8.02–7.96 (m, 4H), 7.70–7.65 (m, 1H), 7.55–7.51 (m, 2H), 7.02–6.99 (m, 2H), 3.91 (s, 3H); ¹³C-NMR (CDCl_3 , 100 MHz): δ 194.9, 193.2, 165.0, 134.8, 133.2, 132.4, 129.9, 129.0, 126.1, 114.4, 55.7; IR (KBr cm^{-1}): 3065, 2935, 2843, 1671, 1597, 1510, 1453, 1314, 1264, 1167, 1024, 879, 842, 758, 718, 684. Anal. Calcd for $\text{C}_{15}\text{H}_{12}\text{O}_3$ (240.25): C, 74.99; H, 5.03. Found: C, 75.07; H, 5.13.

4 | RESULT AND DISCUSSION

As can be seen in Schemes 1 and 2, our magnetic catalytic system was prepared in several steps (for details see Experimental section).

Prepared catalyst was then characterized using various microscopic and spectroscopic techniques such as, FT-IR, VSM, ICP, TGA, SEM-EDX and TEM. FT-IR spectra of the synthesized samples are depicted in Figure 1. In the spectrum in Figure 1(a), corresponding to the magnetite nanoparticles coated with silica, the signals at 560 and around 1000–1100 cm^{-1} are assigned to the stretching vibrations of Fe–O and Si–O–Si bonds, respectively. In addition, the peak related to the silanol groups has appeared around 3200–3400 cm^{-1} . The FT-IR

**SCHMENE 1** Pathway to preparation of G2



SCHME 2 Synthesis of dendrimer/ruthenium complex

spectrum of $\text{Fe}_3\text{O}_4@\text{SiO}_2-\text{AP}$ is shown in Figure 2(b). In addition to the signals appearing in Figure 1(a), the peak related to the aliphatic C–H bond is visible at 2950 cm^{-1} . In the IR spectra for $\text{Fe}_3\text{O}_4@\text{SiO}_2-\text{AP-TDIC1}$ and $\text{Fe}_3\text{O}_4@\text{SiO}_2-\text{AP-TDIC2}$ (Figures 2c and 2e), the peak at 3200 cm^{-1} can be ascribed to the N–H band stretching frequency. The peak related to the NCO groups has appeared around 2270 cm^{-1} . Also, the observed bonds in the range of $1400\text{--}1600\text{ cm}^{-1}$ and $650\text{--}900\text{ cm}^{-1}$ are related to the stretching vibrations of C–C bonds and out of plane vibrations of C–H aromatic ring, respectively. The broad and strong bonds around $3200\text{--}3400\text{ cm}^{-1}$, related to the hydroxyl groups of pentaerythritol, is well observed in G1 and G2 spectra (Figures 2d and 2f).

Quantitative determination of the organic groups loaded on the surface of magnetite nanoparticles was studied by thermo-gravimetric analysis and elemental analysis (Figure 2 and Table 1). The weight loss of the catalyst between $30\text{--}600\text{ }^\circ\text{C}$ as a function of

temperature was determined using TGA. The TGA plots of $\text{Fe}_3\text{O}_4@\text{SiO}_2-\text{AP}$, $\text{Fe}_3\text{O}_4@\text{SiO}_2-\text{AP-TDIC1}$, G1, $\text{Fe}_3\text{O}_4@\text{SiO}_2-\text{AP-TDIC2}$, and G2 (Figure 2) depict a two-step thermal decomposition. A slight weight loss below $250\text{ }^\circ\text{C}$ corresponds to the removal of physically adsorbed water, whereas, the main weight loss in the second step is due to the removal of organic moieties on the surface. The TGA results are summarized in Table 1. The observed total weight losses for $\text{Fe}_3\text{O}_4@\text{SiO}_2-\text{AP}$, $\text{Fe}_3\text{O}_4@\text{SiO}_2-\text{AP-TDIC1}$, G1, $\text{Fe}_3\text{O}_4@\text{SiO}_2-\text{AP-TDIC2}$, and G2 are 5.76%, 17.68%, 28.72%, 53.75%, and 63.40% respectively. On the basis of these values, the theoretical conversion is 43% for first step, 97% for second step, 78% for third step, and 76% for fourth step. The amount of organic group loaded on the surface of magnetite nanoparticles at each step was calculated based on the TGA data (Table 2). A summary of the elemental analysis is also included in Table 1. As can be seen in this table, a

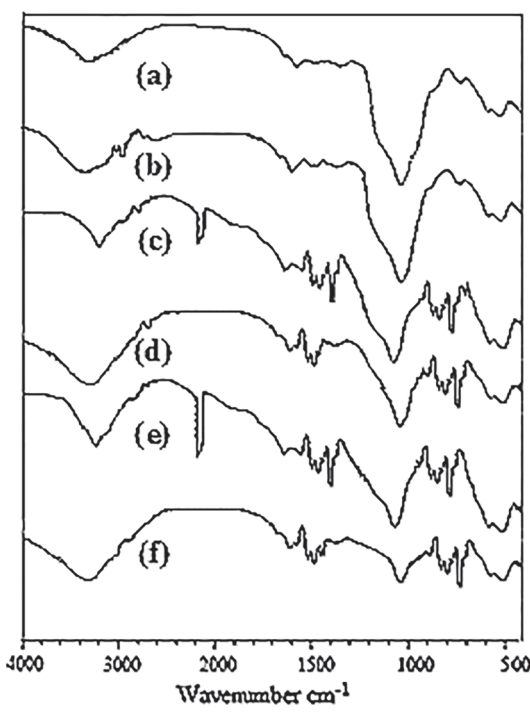


FIGURE 1 FT-IR spectra of (a) $\text{Fe}_3\text{O}_4@\text{SiO}_2$, (b) $\text{Fe}_3\text{O}_4@\text{SiO}_2\text{-AP}$, (c) $\text{Fe}_3\text{O}_4@\text{SiO}_2\text{-AP-TDIC1}$, (d) G1, (e) $\text{Fe}_3\text{O}_4@\text{SiO}_2\text{-AP-TDIC2}$, (f) G2

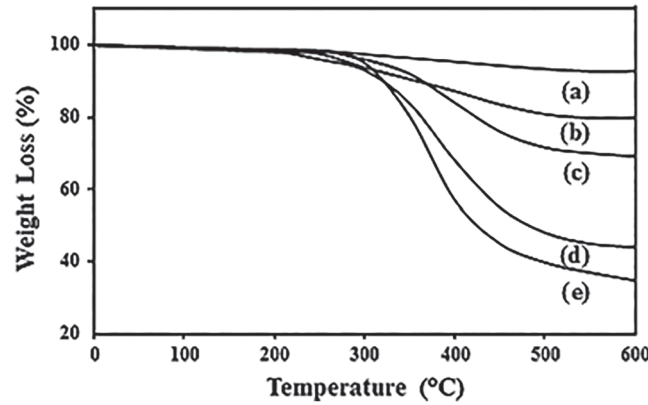


FIGURE 2 Thermogravimetric weight loss plots for the (a) $\text{Fe}_3\text{O}_4@\text{SiO}_2\text{-AP}$, (b) $\text{Fe}_3\text{O}_4@\text{SiO}_2\text{-AP-TDIC1}$, (c) G1, (d) $\text{Fe}_3\text{O}_4@\text{SiO}_2\text{-AP-TDIC2}$, (e) G2

TABLE 2 Thermogravimetric analysis (TGA) results

Sample	Organic (mmol g ⁻¹)	Yield (%)
$\text{Fe}_3\text{O}_4@\text{SiO}_2\text{-AP}$	1	-
$\text{Fe}_3\text{O}_4@\text{SiO}_2\text{-AP-TDIC1}$	0.43	43
G1	0.42	97
$\text{Fe}_3\text{O}_4@\text{SiO}_2\text{-AP-TDIC2}$	0.33	78
G2	0.25	76

good agreement was observed between elemental analysis and TGA data for these conversions.

Magnetic hysteresis measurement for the $\text{Fe}_3\text{O}_4@\text{SiO}_2\text{-CD-Ru}$ (III) was done in an applied magnetic field at r.t., with the field sweeping from -8000 to 8000 Oersted. As shown in Figure 3, the M (H) hysteresis loop for the sample was completely reversible, showing that the nanoparticles exhibited superparamagnetic characteristics. The hysteresis loops reached saturation up to the maximum applied magnetic field. The magnetic saturation value of the catalyst was 25 emu g⁻¹ at r.t.

Nanoparticles morphology was evaluated by Figure 4 SEM (a) and TEM (b) images. Core-shell structure and spherical in shape with a smooth surface morphology of the particles are clearly seen in these images. On the

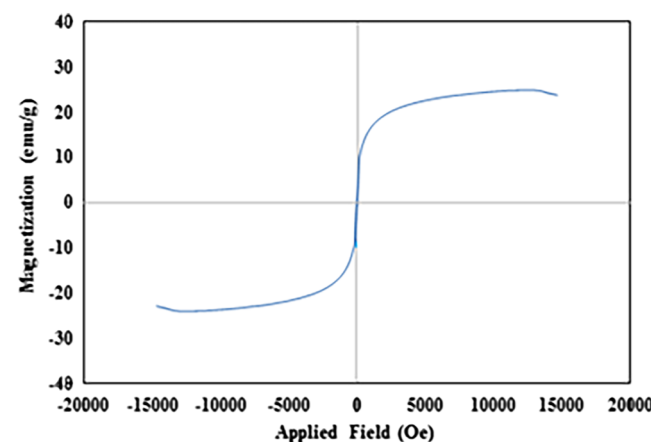


FIGURE 3 VSM curve of the $\text{Fe}_3\text{O}_4@\text{SiO}_2\text{-CD-Ru}$ (III) at r.t

TABLE 1 Elemental analysis and TGA results for the synthesis of catalyst

%	$\text{Fe}_3\text{O}_4@\text{SiO}_2\text{-AP}$		$\text{Fe}_3\text{O}_4@\text{SiO}_2\text{-TDIC1}$		G1		$\text{Fe}_3\text{O}_4@\text{SiO}_2\text{-TDIC2}$		G2	
	EA	TGA	EA	TGA	EA	TGA	EA	TGA	EA	TGA
C	3.70	3.64	10.86	10.97	15.85	15.76	33.40	33.32	34.18	34.27
H	0.76	0.71	1.00	0.87	1.80	1.86	2.74	2.61	3.80	3.82
N	1.52	1.41	3.02	3.05	2.97	2.97	5.47	5.27	5.40	5.86
O	-	-	-	2.79	-	8.13	-	12.55	-	19.45
T	5.98	5.76	17.70	17.68	28.80	28.72	54.18	53.75	62.88	63.40

T: Total weight

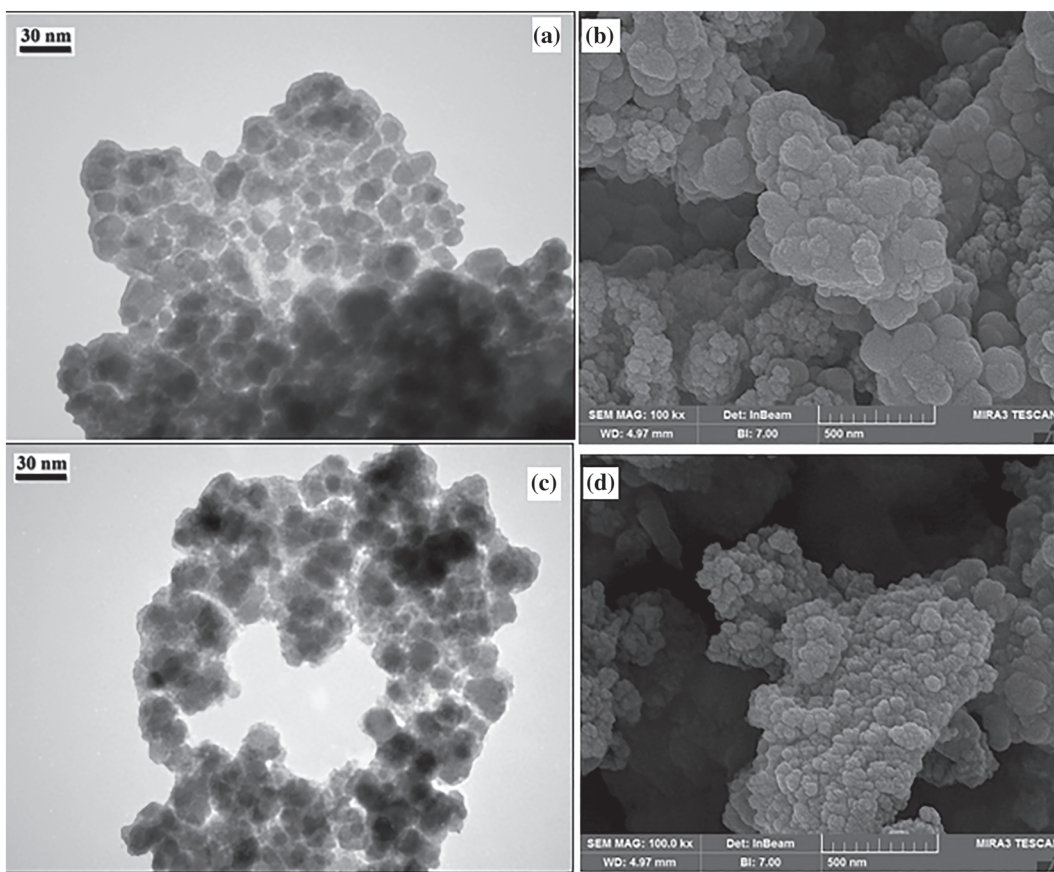


FIGURE 4 TEM and SEM images of $\text{Fe}_3\text{O}_4@\text{SiO}_2\text{-CD-Ru}$ (III) before (a and b) and after (c and d) being reused 15 times

other hand, these images confirm that the particle size is below 30 nm.

A typical way to show the particle size and its distribution is in the form of a number-frequency histogram. Histograms obtained from 100 nanoparticles illustrate the frequency of occurrence versus the size range, the average particle size of $\text{Fe}_3\text{O}_4@\text{SiO}_2\text{-CD-Ru}$ (III) ($25 \text{ nm} \pm 0.5$) were obtained (Figure 5a). To confirm the presence of ruthenium in the catalyst structure energy-dispersive X-ray analysis (EDX) was performed

(Figure 5b). In addition to ruthenium, other atoms such as silicon, oxygen, iron and nitrogen, related to the catalyst structure, are seen in the spectrum.

Ruthenium content of the catalyst was probed by Inductively Coupled Plasma analysis (ICP). For this purpose, the catalyst (50 mg) was dissolved in a mixture of nitric acid and hydrochloric acid (1:3, 20 ml) and after analysis, the amount of the ruthenium loaded on the surface of magnetic nanoparticles was obtained as 0.12 mmol per gram of catalyst.

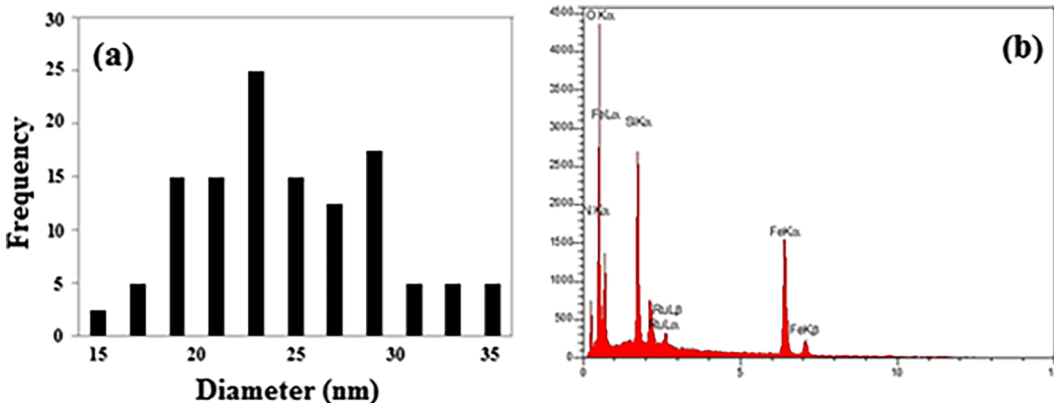


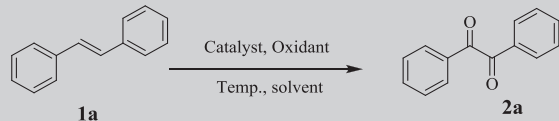
FIGURE 5 histograms generated from the sizes of the $\text{Fe}_3\text{O}_4@\text{SiO}_2\text{-CD-Ru}$ (III) (a), EDX pattern (b)

After characterization of the catalyst structure, its catalytic activity was studied in oxidation reaction of stilbenes to diaryl-1,2-diketones. Oxidation of stilbene to benzil was chosen as the model reaction to find the optimum conditions. The results are summarized in Table 3.

When the model reaction was carried out under the following conditions: TBHP (5 mmol) as oxidant, TBAI (20 mol%) as co-catalyst and solvent-free at room

temperature under air atmosphere for 5 hr, no product was formed (Table 3, entry 1). Employment of $\text{Fe}_3\text{O}_4@\text{SiO}_2$ or $\text{Fe}_3\text{O}_4@\text{SiO}_2\text{-CD}$ (5 mg) as catalyst did not have an effect on the progression of the reaction too (Table 3, entries 2 and 3). Formation of product **2a** with 85% yield after 1 hr of the reaction time in the presence of the $\text{Fe}_3\text{O}_4@\text{SiO}_2\text{-CD-Ru}$ (III) (5 mg, 0.06 mol% of Ru) as catalyst shown that the Ru play a vital role for this

TABLE 3 Screening the reaction conditions^a



Entry	Catalyst (mg)	Oxidant	Co-catalyst	Solvent	Time (hr)	Yield (%) ^b
1	-	TBHP	TBAI	-	5	-
2	$\text{Fe}_3\text{O}_4@\text{SiO}_2$ (5)	TBHP	TBAI	-	5	-
3	$\text{Fe}_3\text{O}_4@\text{SiO}_2\text{-CD}$ (5)	TBHP	TBAI	-	5	-
4	$\text{Fe}_3\text{O}_4@\text{SiO}_2\text{-CD-Ru}$ (III) (5)	TBHP	TBAI	-	1	85
5	$\text{Fe}_3\text{O}_4@\text{SiO}_2\text{-CD-Ru}$ (III) (4)	TBHP	TBAI	-	1	80
6	$\text{Fe}_3\text{O}_4@\text{SiO}_2\text{-CD-Ru}$ (III) (6)	TBHP	TBAI	-	1	85
7	$\text{Fe}_3\text{O}_4@\text{SiO}_2\text{-CD-Ru}$ (III) (5)	-	TBAI	-	5	-
8	$\text{Fe}_3\text{O}_4@\text{SiO}_2\text{-CD-Ru}$ (III) (5)	H_2O_2	TBAI	-	5	-
9	$\text{Fe}_3\text{O}_4@\text{SiO}_2\text{-CD-Ru}$ (III) (5)	DTBP	TBAI	-	5	-
10	$\text{Fe}_3\text{O}_4@\text{SiO}_2\text{-CD-Ru}$ (III) (5)	NaOCl	TBAI	-	5	-
11	$\text{Fe}_3\text{O}_4@\text{SiO}_2\text{-CD-Ru}$ (III) (5)	$\text{PhI}(\text{OAc})_2$	TBAI	-	5	-
12 ^c	$\text{Fe}_3\text{O}_4@\text{SiO}_2\text{-CD-Ru}$ (III) (5)	TBHP	TBAI	-	2	75
13 ^d	$\text{Fe}_3\text{O}_4@\text{SiO}_2\text{-CD-Ru}$ (III) (5)	TBHP	TBAI	-	1	85
14	$\text{Fe}_3\text{O}_4@\text{SiO}_2\text{-CD-Ru}$ (III) (5)	TBHP	-	-	5	-
15	$\text{Fe}_3\text{O}_4@\text{SiO}_2\text{-CD-Ru}$ (III) (5)	TBHP	I_2	-	5	-
16	$\text{Fe}_3\text{O}_4@\text{SiO}_2\text{-CD-Ru}$ (III) (5)	TBHP	TBAB	-	5	-
17	$\text{Fe}_3\text{O}_4@\text{SiO}_2\text{-CD-Ru}$ (III) (5)	TBHP	Bu_4NCl	-	5	-
18 ^e	$\text{Fe}_3\text{O}_4@\text{SiO}_2\text{-CD-Ru}$ (III) (5)	TBHP	TBAI	-	1	70
19 ^f	$\text{Fe}_3\text{O}_4@\text{SiO}_2\text{-CD-Ru}$ (III) (5)	TBHP	TBAI	-	1	85
20	$\text{Fe}_3\text{O}_4@\text{SiO}_2\text{-CD-Ru}$ (III) (5)	TBHP	TBAI	EtOAc	3	40
21	$\text{Fe}_3\text{O}_4@\text{SiO}_2\text{-CD-Ru}$ (III) (5)	TBHP	TBAI	Toluene	1	60
22	$\text{Fe}_3\text{O}_4@\text{SiO}_2\text{-CD-Ru}$ (III) (5)	TBHP	TBAI	CH_3CN	1	60
23	$\text{Fe}_3\text{O}_4@\text{SiO}_2\text{-CD-Ru}$ (III) (5)	TBHP	TBAI	<i>n</i> -hexane	3	20
24	$\text{Fe}_3\text{O}_4@\text{SiO}_2\text{-CD-Ru}$ (III) (5)	TBHP	TBAI	H_2O	1	80
25 ^e	$\text{Fe}_3\text{O}_4@\text{SiO}_2\text{-CD-Ru}$ (III) (5)	TBHP	TBAI	-	1	70
26	CD-Ru (III) complex	TBHP	TBAI	-	1	85

^aReaction conditions: stilbene (1 mmol), oxidant (5 mmol), co-catalyst (20 mol%), solvent (2 ml), under air atmosphere

^bThe yields refer to the isolated pure products

^c4 and 6 mmol of TBHP was used, respectively

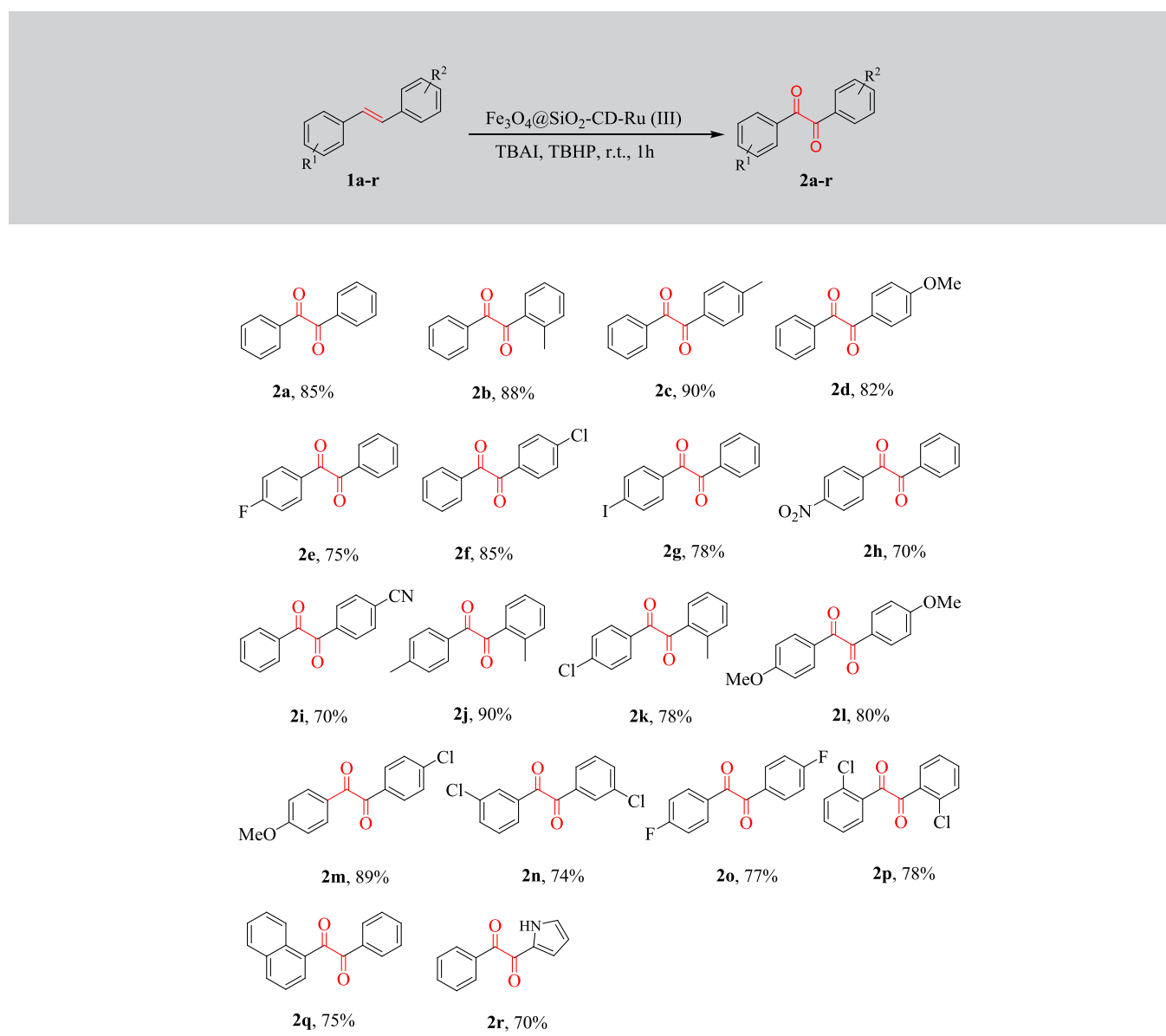
^d10 and 30 mol% of TBAI was used, respectively

^ePerforming the reaction at 60 °C.

transformation (Table 3, entry 4). The 5 mg of catalyst, used in row 4, was also optimized, as the product yield did not change by increasing the amount of catalyst to 6 mg, and by reducing the amount of catalyst to 4 mg, the efficiency was reduced to 80% (Table 3, entries 5 and 6). Next, the effect of oxidant on the yield of the reaction was taken into account. Hence the reaction was carried out in the presence of several oxidizing reagents, such as H_2O_2 , DTBP, NaOCl, and PhI (OAc)₂ as well as attempted in oxidant-free conditions. But in neither case, the benzil was formed (Table 3, entries 7–11). This shows that the presence and type of oxidant are important for this reaction. The amount of oxidant also affected the reaction efficiency. When 4 mmol of oxidant was used,

the efficiency decreased to 75%, although the increase in the amount of oxidant did not result in higher efficiency (Table 3, entries 12 and 13). Almost identical results were obtained in the case of TBAI as auxiliary catalyst. No product formation in the absence of TBAI or in the presence of I_2 , TBAB, and Bu_4NCl showed the importance of TBAI for this reaction (Table 3, entries 14–17). Increasing the amount of TBAI to 30 mol% made no difference to the reaction yield. Conversely, the reduction in catalyst loading to 10 mol% gave rise to a drop in yield (Table 3, entries 18 and 19). The effect of solvent was also studied. For this propose, some organic solvents as well as H_2O were examined but none of them had the effect of solvent-free conditions. (Table 3, entries 20–24). The

TABLE 4 The structures of the synthesized diaryl-1,2-diketones^a



Reaction conditions: 1,2-diaryl ethene (1 mmol), catalyst (5 mg, 0.06 mol% of Ru), TBAI (20 mol%), TBHP (5 equiv), r.t., under air atmosphere. The yields refers to the isolated pure products.

increase in temperature also had a negative effect on the yield of the product, and at 60 °C, the product achieved with 70% yield (Table 3, entry 25). Although the ruthenium-dendrimer complex also performed these transformations well (Table 3, entry 26), easy separation, by using an external magnet, and high reusability, up to fifteenth times, are two salient features of this complex fixed on the surface of magnetic nanoparticle.

To evaluate the activity of $\text{Fe}_3\text{O}_4@\text{SiO}_2$ -CD-Ru (III) in the synthesis of other 1,2-diketones by this method, various 1,2-diaryl ethene derivatives were subjected to the reaction conditions (Table 4). Under the standard reaction conditions, various 1,2-diaryl ethene derivatives having different functional groups on aromatic rings were well converted to the corresponding 1,2-diketones at short reaction time in good to high yields. Generally speaking, those having electron-donating groups on the aromatic ring has a better efficiency than that of electron-withdrawing groups. Moreover, 1-styryl naphthalene, a polycyclic stilbene, and 2-styryl-1H-pyrrole were oxidized to the corresponding 1,2-diketones with good efficiency.

The aim of stabilizing the catalytic core on the surface of magnetic nanoparticles was its easy magnetic separation, recovery, and reusability. For this purpose and after completion of the reaction in the first run at the model reaction, the catalyst was easily separated from the reaction mixture by using an external magnet; it was washed with ethyl acetate (3×10 ml), dried at 60 °C and immediately used in the next step. The reaction was repeated for up to 15 consecutive runs without significant change in the efficiency of the catalyst (Scheme 3).

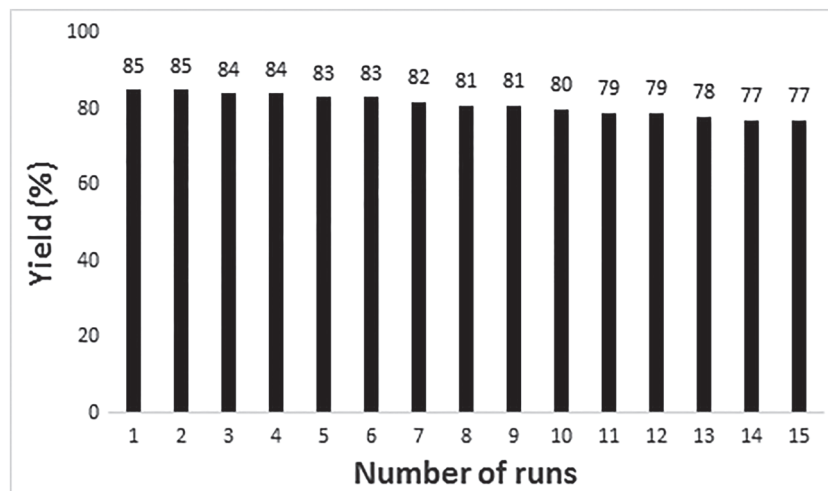
Also, the obtained ICP-OES data from the reused catalyst (after recycling fifteenth times) show that only a low amount of Ru nanoparticles (<1%) are lost from the surface of magnetic nanoparticles during reaction process. So, these results confirmed that the $\text{Fe}_3\text{O}_4@\text{SiO}_2$ -

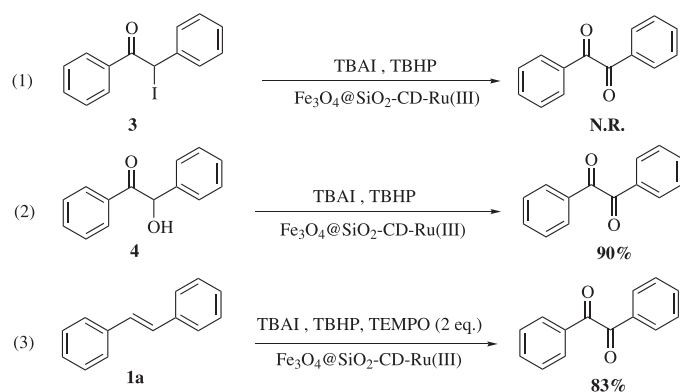
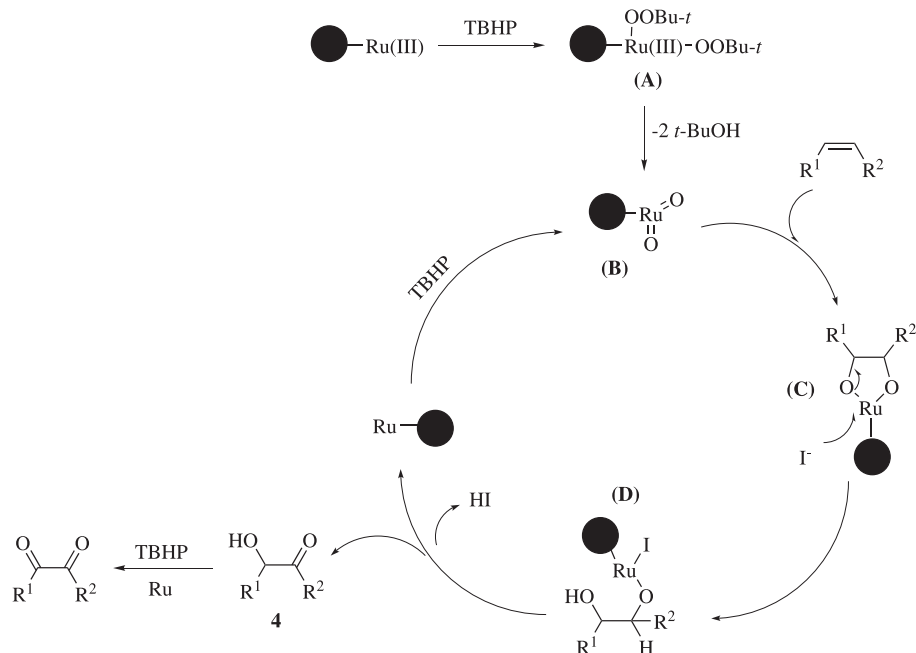
CD-Ru (III) catalyst provides the high catalytic activity, and not any leached Ruthenium. Moreover, the TEM and SEM images of the catalyst showed that the morphology and size of the catalyst after recycling fifteenth times does not change significantly (Figure 4c and 4d).

A series of control experiments was performed on the model reaction to study the reaction mechanism. It has previously been shown that without the presence of TBAI, no product is formed (Table 3, entry 14). The oxidation of alpha-iodo ketone **3**, which is thought to be one of the reaction intermediates, was evaluated. Contrary to expectation, the product did not form, which indicates that the **3** is not intermediate in the pathway for the reaction (Scheme 4, Equation 1). In order to prove the presence of alpha-hydroxy ketone **4** as an intermediate, benzoin was subjected to the optimized reaction conditions and benzil obtained with 83% yield. This showed that benzoin **4** could be an intermediate in this reaction (Scheme 4, Equation 2). Moreover, in the presence of 2,2,6,6-tetra-methylpiperidine-N-oxyl (TEMPO), a well-known radical scavenger, the model reaction was not hampered and no TEMPO-bound intermediate was observed. This shows that the transformation may not involve a radical pathway (Scheme 4, Equation 3).

On the basis of our experimental observation and precedent reports,^[6e, f, 11] a possible mechanism as outlined in scheme 5 was proposed for this oxidative transformation. First, the intermediate **A** is formed, by the reaction of TBHP with Ru (III), which is then converted to intermediate **B**, by the loss of two molecules of *t*-BuOH. Intermediate **C** is formed through a [3 + 2] cycloaddition reaction between **B** and the alkene. The nucleophilic attack of iodide on ruthenium of intermediate **C**, affords intermediate **D** which then undergoes β -hydrogen elimination, leading to α -hydroxyl ketone **4**, and the subsequent oxidation of **4** would produce the desired α -diketone.

SCHEME 3 Recycling of the catalyst in the model reaction carried out for 1 hr



**SCHEME 4** Control experiment to understand the reaction mechanism**SCHEME 5** Plausible reaction mechanism

For comparison, the efficacy of several catalytic systems as well as the present magnetic catalyst, view the point of reaction conditions, time, efficiency, and ultimately turnover frequency, is illustrated in Table 5 for

the synthesis of benzil. As can be seen in this table, our magnetic catalytic system performs this transformation in the short reaction time with high TOF under the mild reaction conditions. In addition, the catalyst is easily

TABLE 5 Comparison of different catalysts in the conversion of stilbene to benzil^a

Entry	Catalyst (mol%)	Time (h)	Yield (%)	TOF (h ⁻¹)	Ref.
1	[Ru (cymene)Cl ₂] ₂ (1)	1	91	91	[6e]
2	I ₂ (2 equiv)	20	96	-	[6g]
3 ^b	[Ru (cymene)Cl ₂] ₂ (0.001)	12	93	7750	[6h]
4 ^b	RuCl ₃ ·3H ₂ O (0.5)	2	82	82	[6k]
5 ^b	Pd-Fe ₃ O ₄ (1)	28	98	3.5	[6i]
7 ^c	Fe ₃ O ₄ @SiO ₂ -CD-Ru (III) (0.06)	1	85	1417	Present work

^aConditions: For entries: (1) TBAI, TBHP, toluene/MeCN/H₂O, r.t.; (2) H₂O, 140 °C; (3) I₂, dioxane, 80 °C; (4) Diethylcarbonate, NaOCl, r.t.; (5) CuBr₂, 1,4-dioxane/H₂O, 95 °C

^b1,2-Diphenylacetylene has compared instead of stilbene

^cReusability of the catalyst is ignored to calculate the TOF.

separated from the reaction medium, and exhibits high reusability (up to 15 times).

5 | CONCLUSION

We developed a novel and alternative route to catalyze oxidation reaction of alkenes. To this end, ruthenium/dendrimer complex immobilized on silica-functionalized magnetite nanoparticles was prepared and its catalytic activity was explored in the synthesis of benzil derivatives via the oxidation of 1,2-diaryl ethenes. The synthesized catalytic system could catalyze these transformations in short reaction time with a high TOF. Straightforward separation, remarkable aptitude to be recycled up to fifteen times and good stability are all salient features of this catalytic system.

ACKNOWLEDGMENTS

We are thankful to Persian Gulf University Research Council for partial support of this work.

ORCID

Dariush Saberi  <https://orcid.org/0000-0003-1844-7815>

Majid Moghadam  <https://orcid.org/0000-0001-8984-1225>

Khodabakhsh Niknam  <https://orcid.org/0000-0001-5742-3846>

REFERENCES

- [1] a)M. R. Angelastro, S. Mehdi, J. P. Burkhardt, N. P. Peet, P. Bey, *J. Med. Chem.* **1990**, *33*, 11. b)K. C. Nicolaou, D. L. F. Gray, J. Tae, *J. Am. Chem. Soc.* **2004**, *126*, 613. c) M. D. Rozwadowska, M. Chrzanowska, *Tetrahedron* **1985**, *41*, 2885. d)S. E. Wolkenberg, D. D. Wisnoski, W. H. Leister, Y. Wang, Z. Zhao, C. W. Lindsley, *Org. Lett.* **2004**, *6*, 1453. e) A. J. Herrera, M. Rondon, E. Suarez, *J. Org. Chem.* **2008**, *73*, 3384. f)X. Deng, N. S. Mani, *Org. Lett.* **2006**, *8*, 269. g) G. R. Boyce, J. S. Johnson, *Angew. Chem. Int. Ed.* **2010**, *49*, 8930. *Angew. Chem.* **2010**, *122*, 9114
- [2] L. Benhamou, E. Chardon, G. Lavigne, S. Bellemain-Laponnaz, V. César, *Chem. Rev.* **2011**, *111*, 2705.
- [3] a)B. I. Ita, O. E. Offiong, *Mater. Chem. Phys.* **2001**, *70*, 330. b) T. Harada, Y. Nakagawa, R. M. Wadkins, P. M. Potter, C. E. Wheelock, *Bioorg. Med. Chem.* **2009**, *17*, 149. c) C. D. Fleming, S. Bencharit, C. C. Edwards, J. Hyatt, L. Tsurkan, F. Bai, C. Fraga, C. L. Morton, E. L. Howard-Williams, P. M. Potter, M. R. Redinbo, *J. Mol. Biol.* **2005**, *352*, 165.
- [4] a)B. Husár, S. Commereuc, I. Lukáć, S. Chmela, J. M. Nedelec, M. Baba, *J. Phys. Chem. B* **2006**, *110*, 5315. b)T. Corrales, F. Catalina, C. Peinado, S. N. Allen, *J. Photochem. Photobiol. A* **2003**, *159*, 103.
- [5] a)C. Mousset, A. Giraud, O. Provot, A. Hamze, J. Bignon, J. M. Liu, S. Thoret, J. Dubois, D. J. Brion, M. Alami, *Bioorg. Med. Chem. Lett.* **2008**, *18*, 3266. b)S. Ganapaty, G. V. K. Srilakshmi, S. T. Pannakal, H. Rahman, H. Laatsch, R. Brun, *Phytochemistry* **2009**, *70*, 95.
- [6] a)A. Tymonko, B. A. Nattier, R. S. Mohan, *Tetrahedron Lett.* **1999**, *40*, 7657. b)M. Shaikh, M. Satanami, K. V. S. Ranganath, *Cat. Com.* **2014**, *54*, 91. c)M. Kirihara, Y. Ochiai, S. Takizawa, H. Takahata, H. Nemoto, *Chem. Commun.* **1999**, 1387. d)Y. Su, L. Zhang, N. Jiao, *Org. Lett.* **2011**, *13*, 2168. e)S. Chen, Z. Liu, E. Shi, L. Chen, W. Wei, H. Li, Y. Cheng, X. Wan, *Org. Lett.* **2011**, *13*, 2274. f)H. P. Jia, D. R. Dreyer, C. W. Bielawski, *Tetrahedron* **2011**, *67*, 4431. g)X. Zeng, C. Miao, S. Wang, C. Xia, W. Sun, *RSC Adv.* **2013**, *3*, 9666. h)W. Ren, J. Liu, L. Chen, X. Wan, *Adv. Synth. Catal.* **2010**, *352*, 1424. i)S. Byun, J. Chung, T. Lim, J. Kwon, M. Kim, *RSC Adv.* **2014**, *4*, 34084. j) A. Gao, F. Yang, J. Li, Y. Wu, *Tetrahedron* **2012**, *68*, 4950. k) Y. Miao, A. Dupé, C. Bruneau, C. Fischmeister, *Eur. J. Org. Chem.* **2014**, 5071. l)W. Ren, Y. Xia, S. J. Ji, Y. Zhang, X. Wan, J. Zhao, *Org. Lett.* **2009**, *11*, 1841. m)C. F. Xu, M. Xu, Y. X. Jia, C. Y. Li, *Org. Lett.* **2011**, *13*, 1556. n)Z. Wan, C. D. Jones, D. Mitchell, J. Y. Pu, T. Y. Zhang, *J. Org. Chem.* **2006**, *71*, 826. o)D. Villemin, M. Hammadi, *Synth. Commun.* **1995**, *25*, 3145. p)S. Verma, J. L. Bras, S. L. Lain, J. Muzart, *Appl. Catal. A* **2013**, *468*, 334. q)J. M. Khurana, B. M. Kandpal, *Tetrahedron Lett.* **2003**, *44*, 4909. r)C. Qi, H. Jiang, L. Huang, Z. Chen, H. Chen, *Synthesis* **2011**, 387. s)J. C. Lee, H. J. Park, J. Y. Park, *Tetrahedron Lett.* **2002**, *43*, 5661. t)Z. Li, J. Yin, G. Wen, T. Li, X. Shen, *RSC Adv.* **2014**, *4*, 32298. u)X. Wang, G. Cheng, J. Shen, X. Yang, M. Wei, Y. Feng, X. Cui, *Org. Chem. Front.* **2014**, *1*, 1001. v)A. Wang, H. Jiang, X. Li, *J. Org. Chem.* **2011**, *76*, 6958. w)W. Yang, Y. Chen, Y. Yao, X. Yang, Q. Lin, D. Yang, *J. Org. Chem.* **2019**, *84*, 11080. x)S. W. Kim, T.-W. Um, S. Shin, *J. Org. Chem.* **2018**, *83*, 8703. y)A. H. Bansode, G. Suryavanishi, *ACS Omega* **2019**, *4*, 9636.
- [7] a)H. Min, T. Palani, K. Park, J. Hwang, S. Lee, *J. Org. Chem.* **2014**, *79*, 6279. b)J. B. Bharate, S. Abbat, R. Sharma, P. V. Bharatam, R. A. Vishwakarma, S. B. Bharate, *Org. Biomol. Chem.* **2015**, *13*, 5235. c)W. X. Lv, Y. F. Zeng, S. S. Zhang, Q. Li, H. Wang, *Org. Lett.* **2015**, *17*, 2972. d)Y. Su, X. Sun, G. Wu, N. Jiao, *Angew. Chem. Int. Ed.* **2013**, *52*, 9808. *Angew. Chem.* **2013**, *125*, 9990 e)D. Saberi, H. Hashemi, K. Niknam, *Asian J. Org. Chem.* **2017**, *6*, 169. f) A.-M. D. Schmitt, M. R. Garnsey, H. M. Wisniewska, J. I. Murray, T. Lee, D. W. Kung, N. Sach, D. G. Blackmond, *ACS Catal.* **2019**, *9*, 4508. g)R. K. Vishwakarma, S. Kumar, A. K. Sharma, R. Singh, K. N. Singh, *Chemistry Select* **2019**, *4*, 4064.
- [8] a)D. A. Tomalia, *Adv. Mater.* **1994**, *6*, 529. b)G. R. Newkome, C. N. Morrefield, F. Vogtle, *Dendritic Molecules: Concepts, Syntheses, Perspectives*, VCH, Weinheim, Germany **1996**. c)F. Zeng, S. C. Zimmerman, *Chem. Rev.* **1997**, *97*, 1681. d)J. S. Moore, *Acc. Chem. Res.* **1997**, *30*, 402. e) O. A. Mathews, A. N. Shipway, J. F. Stoddart, *Prog. Polym. Sci.* **1998**, *23*, *1*. f)H. Frey, C. Lach, K. Lorenz, *Adv. Mater.* **1998**, *10*, 279. g)C. Gorman, *Adv. Mater.* **1998**, *10*, 295. h) J. M. Fréchet, *J. Sci.* **1994**, *263*, 1710. i)M. Akisada, R. Kimura, Y. Tachi, S. Suzuki, K. Okada, M. Kozaki, *J. Org. Chem.* **2018**, *83*, 9631. j)H. Xiao, R. Wang, L. Dong, Y. Cui, S. Chen, H. Sun, G. Ma, D. Gao, L. Wang, *ACS Omega* **2019**, *4*, 18685. k) Y. Inomata, K. Albrecht, N. Haruta, K. Yamamoto, *Chem.*

- Mater. **2019**, *31*, 8373. l)K. Zheng, J. Ren, J. He, *Macromolecules* **2019**, *52*, 6780.
- [9] Q. Du, W. Zhang, H. Ma, J. Zheng, B. Zhou, Y. Li, *Tetrahedron* **2012**, *68*, 3577.
- [10] C. Pereira, A. M. Pereira, P. Quaresma, P. B. Tavares, E. Pereira, J. P. Araujo, C. Freire, *Dalton Trans.* **2010**, *39*, 2842.
- [11] a)S.-I. Murahashi, T. Naota, K. Yonemura, *J. Am. Chem. Soc.* **1988**, *110*, 8256. b)S.-I. Murahashi, N. Komiya, Y. Oda, T. Kuwabara, T. Naota, *J. Org. Chem.* **2000**, *65*, 9186. c)M.-Z. Wang, C.-Y. Zhou, M.-K. Wong, C.-M. Che, *Chem. – Eur. J.* **2010**, *16*, 5723.

How to cite this article: Saberi D, Hashemi H, Ghanaatzadeh N, Moghadam M, Niknam K. Ruthenium/dendrimer complex immobilized on silica-functionalized magnetite nanoparticles catalyzed oxidation of stilbenes to benzil derivatives at room temperature. *Appl Organometal Chem.* 2020;e5563. <https://doi.org/10.1002/aoc.5563>